Li-insertion/extraction properties of three-dimensional Sn electrode prepared by facile electrodeposition method

Masahiro Shimizu[a,b], *Mendsaikhan Munkhbat*[a], *and Susumu Arai*[a,b*]

[a] *Department of Materials Chemistry, Faculty of Engineering, Shinshu University, 4-17-1 Wakasato, Nagano, 380-8553, Japan*

[b] *Institute of Carbon Science and Technology, Faculty of Engineering, Shinshu University, 4-17-1 Wakasato, Nagano, 380-8553, Japan*

Prof. Masahiro Shimizu
E-mail: shimizu@shinshu-u.ac.jp
Tel: +81-26-269-5627; Fax: +81-26-269-5627

Prof. Susumu Arai (*Corresponding author)
E-mail: araisun@shinshu-u.ac.jp
Tel: +81-26-269-5413; Fax: +81-26-269-5432

ABSTRACT

Toward the realization of reliable Li-ion batteries with high performance and safety, component materials such as those of the current collector and negative electrode require further innovation. Sn, one of the most promising negative-electrode materials, can be electrochemically fixed on a substrate without any binder or conductive additive. However, the pulverization of Sn-plating films on substrates caused by large volume changes during Li–Sn reactions is the main reason hindering the practical application of Sn-plated electrodes. In the present study, we developed an electrodeposited three-dimensional (3D) Cu substrate applied to underlayer of the electrode. The effect of substrate geometry on the charge–discharge performance of the Sn electrode was investigated. The 3D-Cu/Sn electrode exhibited superior cycling performance with a reversible capacity of 470 mA h g^{-1} even at the 300th cycle, whereas the Sn-plated electrode prepared on a typical flat Cu substrate showed a capacity of only 20 mA h g^{-1}. The results demonstrated that the 3D structure played a key role in accommodating volumetric changes in the Sn to suppress electrode disintegration. The developed 3D-Cu substrate will be significantly useful as a current collector for alloy-based active materials.

KEYWORDS:

Electrodeposition; Sn electrode; Li-ion battery; Three-dimensional structure; Current collector

1. Introduction

The use of tin (Sn) as a negative electrode material is one of the solutions for the realization of Li-ion batteries with high-energy density because of its theoretical capacity of 993 mA h g^{-1} [1-3]. Furthermore, its specific gravimetric and volumetric capacity (7313 mA h cm^{-3}) are much larger than those of the currently used graphite (LiC_6: 372 mA h g^{-1}, 883 mA h cm^{-3}) [4]. Sn has an excellent electronic conductivity in comparison with that of silicon, which is also expected to be a promising candidate owing to its high theoretical capacity [5,6]. Additionally, a Sn active material layer can be simply and directly fixed on a substrate by electrodeposition method without any binder or conductive additive, unlike general preparation methods [3]. The construction of a Sn film by electroplating, however, causes a critical cyclability. The electrodeposited layer is too dense to accommodate volume changes in the Sn during alloying and dealloying reactions with Li, and thereby results in electrode disintegration such as pulverization of the Sn, which causes capacity fading. Sn undergoes a significant volume expansion of up to 260% (difference between Sn and $Li_{22}Sn_5$) upon complete lithiation [4]. In view of this large volume expansion ratio, to achieve a high reversible capacity over long operating periods, the introduction of buffer layer which can accommodate volume changes derived from Li–Sn reactions into the electrode structure is considered to be an effective approach. As another strategy, the application of Sn-based intermetallic compounds M_xSn_y (e.g. M=transition metal) is significantly effective for enhancement of electrode performance [7-11]. M_xSn_y undergoes a phase separation to form metallic Sn in an initial charge process. An inactive M acts as a buffer to release a stress induced by Li–Sn alloying reactions, and thereby lead to good performance. Kanamura et al reported the design of Ni-Sn alloy electrode with three-dimensional (3D) structure prepared by using a colloidal crystal templating process coupled with an electroplating on a flexible Cu current collector

patterned with photoresist substrate, and achieved a high cyclability in the Sn-based electrode [12]. On the other hand, the use of porous Cu substrate as a current collector is also cited as a typical approach [13,14]. Porous substrates with a 3D structure and emphasized anchor effect can improve electrical contact [7] and adhesiveness [10] between the active material layer and substrate to enhance electrode performance. However, the preparation of such structures is generally carried out using a top-down type approach and so requires a plurality of steps such as dissolution or dealloying of one side of the metal from a bimetallic sintered compact [15,16]. Although there is another approach that uses a blowing agent like a water-soluble polymer binder, this technique requires high temperature and controlled pressure conditions [17,18]. Sun et al applied an electroless plating method to fabrication of 3D porous Cu films for the first time, and demonstrated that such a configuration can be easily prepared [19]. The Sn-Co alloy deposited on the 3D films maintained a reversible capacity more than 500 mA h g^{-1} with a capacity retention of 83% after 70 cycles. The 3D porous structure suppressed the exfoliation of the active material layer from the current collector. In our previous study, we found that a 3D Cu structure could be fabricated by electrodeposition even at ordinary temperature and pressure just by adding a certain organic additive to the electroplating bath [20]. Our developed method is highly productive as well as a bottom-up type approach. The 3D Cu substrate is composed of a Cu nano-sheet grown on the underlayer, and forms an interspace inside itself. The internal space and roughened surface are considered to accommodate the volumetric change of Sn and suppress the disintegration of the Sn film on the substrate. Electrodeposition of Sn on this substrate allows the preparation of a current collector-integrated negative-electrode without any binder or conductive additive. Furthermore, coating a slurry containing an active material on the substrate will yield an adhesion-reinforced mixed electrode. In either case, the unique structure is expected to be effective in exerting the

potential high capacity of active materials. In the present study, we conducted Sn electroplating on 3D-Cu substrate, and investigated the influence of substrate morphology on its Li-insertion/extraction properties as a negative electrode for Li-ion batteries.

2. Experimental

A three-dimensional (3D) Sn electrode was prepared by a facile electrodeposition method. The synthetic conditions of this method were optimized in our previous study [20]. 3.0×10^{-4} mol dm^{-3} (M) polyacrylic acid [PAA; Wako Pure Chemical Industries, Ltd., average molecular weight (A.M.W.): 5000], which is a 3D structure former, was added to an electroplating bath containing an aqueous solution of 0.85 M copper (II) sulfate ($CuSO_4$; 99.5%) and 0.55 M sulfuric acid (H_2SO_4). A 3D-Cu structure was fabricated on a Cu-foil (3×3.3 cm^2) by electroplating using the solution under galvanostatic conditions at 298 K without stirring. The current density and Coulomb was 1.0 A dm^{-2} and 38C, respectively. The resulting 3D-Cu substrate was immersed in a Sn plating bath composed of 0.25 M tin (II) pyrophosphate ($Sn_2P_2O_7$; 95.0%), 1.0 M potassium pyrophosphate ($K_4P_2O_7$; 98.0%), 0.002 M polyethylene glycol (PEG; A.M.W.: 600), and 0.005 M formaldehyde (HCHO). The 3D-Cu/Sn electrode was fabricated by electrodeposition of Sn with a charge amount of 3C (=3.7 mg). The loading mass of Sn per square centimeter correspond approximately to 0.37 mg cm^{-2}. To reveal the influence of substrate morphology on electrode performance, a flat Cu substrate was also used. The condition of the Sn plating such as bath composition and charge amount is same as for preparation of the 3D-Cu/Sn.

The crystal structure of the film plated on the Cu substrate was identified by X-ray diffraction (XRD; SmartLab, Rigaku). The surface and cross-sectional morphology of the electrodes before

and after cycling were observed by a field-emission scanning microscope (FE-SEM; JSM-7000F, JEOL Ltd.) equipped with an energy dispersive X-ray spectroscope.

We fabricated 2032-type coin cells consisting of the 3D-Cu/Sn electrode as the working electrode, Li foil (99.90%, 1.0-mm thickness; Rare Metallic) as the counter electrode, electrolyte, and a glass fiber filter (Whatman GF/A) as the separator. The electrolyte was 1.0 M $LiPF_6$-dissolved in ethylene carbonate (EC) and diethyl carbonate (DEC) with a volume ratio of 50/50. The Li-storage/extraction properties of the 3D-Cu/Sn as a negative electrode was evaluated by charge–discharge tests using an electrochemical measurement system (HJ-1001 SD8, Hokuto Denko Co., Ltd) in the potential range between 0.02 and 1.50 V vs. Li/Li^+ at 298 K.

Electrochemical impedance spectroscopy (EIS) analysis using a three-electrode type cell was performed at 0.02 V vs. Li/Li^+ in the frequency range of 100 kHz–100 mHz with an amplitude of 5 mV at 298 K. Before the EIS measurement, the electrode was charged (lithiated) up to 0.02 V vs. Li/Li^+ at 0.5C (*ca*. 500 mA g^{-1}), and then held at this potential for 20 min.

3. Results and discussion

Figure 1a shows the preparation scheme of the three-dimensional (3D) Cu/Sn electrode by the electrodeposition method. A 3D Cu structure can be simply fabricated on a substrate just by adding polyacrylic acid (PAA), with the obtained surface roughness strongly dependent on the PAA concentration. Additionally, the current density during electroplating also affects the number and thickness of Cu nano-sheets that form the interspace (Figure S1). In the present study, the concentration of PAA and current density of electrodeposition were 3.0×10^{-4} M and 1.0 A dm^{-2}, respectively. Figure 1b displays photographs of the Cu-foil before and after construction of the 3D-Cu on the foil, and the Sn deposited 3D-Cu-substrate. After the fabrication of the 3D-Cu, the

surface of the substrate became lusterless, which indicates that the deposited Cu was rough. In fact, the root mean square roughness (R_{rms}) of the film analyzed by confocal laser scanning microscopy (CLSM, VK-8510; Keyence) was 0.835, much larger than that (0.087) before construction of the 3D-Cu (Figure 2). Figure 3 shows Kr adsorption isotherm of the 3D-Cu substrate, and the Brunauer–Emmett–Teller (BET) surface area of the 3D-Cu substrate is 8.63 m^2 g^{-1}. By assuming that the surface of the reference Cu substrate used in the present study is purely flat, the specific area is 0.22 m^2 g^{-1} and much smaller than that of the 3D-Cu. In other words, the higher surface area prepared by an electroplating method is expected to be effective for enhancement of adhesion between substrate and active material layer. In the case of Sn-film formed on a typical flat Cu-foil, the substrate exhibited specular gloss. In contrast, the Sn plated on the 3D-Cu substrate did not show gloss, meaning that the 3D structure was maintained even after Sn deposition. From the XRD patterns (Figure 1c), it is clear that the deposit on the 3D-Cu substrate was β-Sn without any impurities.

Figure 4 shows surface and cross-sectional FE-SEM images of the 3D-Cu before and after Sn deposition. It is apparent that the 3D-struture was maintained even after the deposition of Sn on the substrate, and that the deposition uniformly took place over the entire 3D-structured substrate. The thickness of the Sn film was estimated to be several tens of nanometers.

Galvanostatic charge–discharge tests were conducted at 0.5C rate to explore the effect of the substrate geometry on the electrode performance of the Sn film. Figure 5a compares the initial Li-insertion/extraction properties of the 3D-Cu/Sn and flat-Cu/Sn electrodes. The initial charge (Li-insertion) capacity of the 3D-Cu/Sn and flat-Cu/Sn electrodes was 1320 mA h g^{-1} and 800 mA h g^{-1}, respectively. The irreversible capacity observed at 2.0 V to 0.5 V for the 3D-Cu/Sn electrode is attributed to reductive decomposition of electrolyte induced by the higher-specific surface area

of the electrode. This issue could be resolved using electrolyte additives such as vinylene carbonate (VC) and fluoroethylene carbonate (FEC), which form a surface layer that suppresses excess electrolyte decomposition [21,22]. No additive, however, was used because the present study was focused on the influence of substrate morphology. Although the surface asperity of the 3D-Cu caused a capacity loss in the charge reaction, its structure increased the number of activation sites for Li–Sn reactions, and thereby achieved a larger discharge capacity (840 mA h g^{-1}) than that of flat-Cu/Sn electrode (700 mA h g^{-1}) in the first cycle. In the dQ/dV profile of 3D-Cu/Sn electrode (Figures 5 and 6), the peak at 0.147 V originated from stepwise alloying reactions of Sn with Li. Given the initial reversible capacity of 840 mA h g^{-1}, it is inferred that the alloy phase reached $Li_{4.4}Sn$ at least. The peaks located at 0.52 V, 0.62 V, 0.77 V, and 1.25 V in the discharge curve indicate Li-extraction from $Li_{22}Sn_5$, $Li_{13}Sn_5$, LiSn, and Li_2Sn_5 phases, respectively (Figure S2) [1,4,23]. Impedance measurements were carried out at 0.02 V vs. Li/Li^+ to analyze which parameters governed the charge−discharge performance of the electrodes. In both Nyquist plots, two semicircles in the high frequency region and a straight line with a slope of approximately 45° in the low frequency region were observed. The first semicircle at higher frequency corresponds to the interfacial resistance (R_{if}) associated with Li-ion conduction through the surface layer induced by electrolyte decomposition, while the second semicircle denotes the charge transfer resistance (R_{ct}) of Li–Sn reactions. The straight line in the low frequency region corresponds to the Warburg impedance (Z_w), which is derived from solid-state diffusion of Li in Sn [22,24]. Each resistance was estimated using the equivalent circuit shown in the inset of Figure 7a. In principle, although the resistance should be standardized by the specific surface area of the electrodes, the area of the 3D-Cu/Sn electrode was complex and still unclear. Therefore, we have left the

resistance value unchanged. It was reported that the inverse of the resistances obeys the Arrhenius-type equation [25,26]:

$$\frac{1}{R_{ct}} = A\exp(-\frac{E_a}{RT}) \quad \cdot \cdot \cdot (2)$$

where the symbol A, E_a, R and T denote frequency factor, activation energy, gas constant, and absolute temperature, respectively. The R_{ct} (2.8 Ω) measured at the first cycle for the 3D-Cu/Sn electrode was smaller than that of the flat-Cu/Sn electrode (6.0 Ω), as expected. The number of active site influences the frequency factor. We inferred that the reason for the reduced resistance comes from the higher specific surface area of the 3D-Cu.

Figure 7b shows the dependence of the discharge capacity and coulombic efficiency of the 3D-Cu/Sn and flat-Cu/Sn electrodes on the cycle number. While the flat-Cu/Sn electrode showed a relatively high reversible capacity at the first cycle, the capacity decayed rapidly after the second cycle. This poor cyclability was probably caused by disintegration of the flat-Cu/Sn electrode. Because the underlayer of the flat-Cu/Sn electrode was smooth, the morphology of the Sn film was inevitably affected by the substrate and had a high density. In view of the significantly large volume change from Sn to Li_xSn alloy (x = 3.5/194%, = 4.4/244%) [1,4], it is clear that the flat-Cu/Sn electrode could not accommodate the volume changes occurring inside the electrode. In contrast, the 3D-Cu/Sn electrode exhibited superior cycling performance with a capacity of 470 mA h g^{-1} at the 300th cycle. The 3D structured electrode accommodated the volumetric change of Sn during lithiation *via* the interspace generated between the Cu nano-sheets. This is the reason why the performance of the 3D-Cu/Sn electrode was significantly improved.

FE-SEM observations of the Sn electrodes after cycling (Figure 8) revealed that cracks were generated on the surface of the flat-Cu/Sn electrode after just 20 cycles. When the electrode was

cycled 50 times, disintegration of the Sn film was obvious. These unfavorable phenomena cause damaged to the surface layer formed on the electrode and thereby exposed a new surface of the electrode. As a result, a renewed surface layer was constructed by electrolyte decomposition [5,27]. The decline in coulombic efficiency observed around the 100th cycle was caused by irreversible electrolyte decomposition related to the electrode disintegration. Furthermore, there little active material layer remained after the 100th cycling. Meanwhile, in the case of the 3D-Cu/Sn electrode, the electrode morphology remained unchanged for a period until the 20th cycle. In the subsequent cycles, although slight differences such as strain were observed, the 3D structure was maintained, which suggests a good structural integrity of the 3D-Cu/Sn electrode. These results demonstrated that the 3D structure effectively accommodated the volume changes of the Sn during the lithiation–delithiation reactions. Finally, we evaluated rate performance of the 3D-Cu/Sn and the flat-Cu/Sn electrodes under various current densities. In the rate performance tests from 0.5 C to 10 C, charge was conducted at the same current density of 0.1C. As a result, the 3D-Cu/Sn electrodes exhibited a reversible capacity of 740 mA h g^{-1} with a capacity retention of 86% even at the 10C (Figure 9), whereas the flat-Cu/Sn electrode could not exert its high theoretical capacity. The good performance is probably considered to be due to the high specific surface area of the 3D-Cu. The 3D-Cu structure prepared in the present study should be a very promising candidate current collector not only for electroplated-film electrodes but also for mixed electrode, especially in cases where high-capacity type active materials such as Sn and Si are used [28]. In a future study, we will report the application of 3D-Cu with a unique structure with controllable roughness.

4. Conclusions

A current collector-integrated electrode was simply prepared by direct Sn-deposition on a 3D-Cu substrate, and those electrochemical properties as a negative electrode for Li-ion batteries were investigated. By taking advantage of the 3D structure with high specific area, the electrode exhibited a larger initial reversible capacity than that of a typical Sn-film (flat-Cu/Sn) electrode prepared by electrodeposition. Additionally, the 3D-Cu substrate accommodated the volume changes of Sn during lithiation and delithiation reactions, and enhanced the cycling performance of the electrode by suppressing disintegration of the active material layer. In contrast, the reversible capacity of the flat-Cu/Sn electrode was quickly lost after just a few cycles, and its cyclability became poor. Our results indicate that 3D-Cu substrate is a very promising candidate as a current collector for Li-ion batteries. We are now attempting to apply this substrate to slurry-type composite electrodes for rechargeable batteries, including Li-, Na-, and multivalent ion (Ca-, Mg-, Al-ion) batteries.

Acknowledgments

This work was supported by Grant-in-Aid for Research Activity Start-up (No. 16H06838) and Scientific Research B (No. 26289270) from the Japan Society for the Promotion of Science (JSPS). This work was supported in part by Alumni Association “Wakasatokai” of Faculty of Engineering, Shinshu University. The authors thank Mr. M. Umeki and Ms. M. Ueda for their kind assistance in CLSM measurements.

References

1. Mao O, Turner RL, Courtney IA, Fredericksen BD, Buckett MI, Krause LJ, Dahn JR (1999) Active/Inactive Nanocomposites as Anodes for Li-Ion Batteries. Electrochem Solid-State Lett 2:3−5.

2. Idota Y, Kubota T, Matsufuji A, Maekawa Y, Miyasaka T (1997) Tin-based amorphous oxide: A High-Capacity Lithium-Ion-Storage Material. Science 276:1395−1397.
3. Ui K, Kikuchi S, Kadoma Y, Kumagai N, Ito S (2009) Electrochemical characteristics of Sn film prepared by pulse electrodeposition method as negative electrode for lithium secondary batteries. J Power Sources 189: 224−229.
4. Obrovac MN, Chevrier VL (2014) Alloy Negative Electrodes for Li-Ion Batteries. Chem Rev 114:11444−11502.
5. Shimizu M, Usui H, Suzumura T, Sakaguchi H (2015) Analysis of the Deterioration Mechanism of Si Electrode as a Li-Ion Battery Anode Using Raman Microspectroscopy. J Phys Chem C 119:2975−2982.
6. Usui H, Shimizu M, Sakaguchi H (2013) Applicability of ionic liquid electrolytes to LaSi2/Si composite thick-film anodes in Li-ion battery. J Power Sources 235:29−35.
7. Ke FS, Huang L, Cai JS, Sun SG (2007) Electroplating synthesis and electrochemical properties of microporous Sn–Cu alloy electrode for lithium-ion batteries. Electrochim Acta 52:6741−6747.
8. Hassoun J, Panero S, Simon P, Taberna PL, Scrosati B (2007) High-Rate, Long-Life Ni–Sn Nanostructured Electrodes for Lithium-Ion Batteries. Adv Mater 19:1632–1635.
9. Tan C, Qi G, Li Y, Guo J, Wang X, Kong D, Wang H, Zhang S (2012) Sn-Cu Alloy Materials with Optimized Nanoporous Structure and Enhanced Performance for Lithium-Ion Batteries Prepared by Dealloying. Int. J Electrochem Sci 7:10303–10312.
10. Ke FS, Huang L, Wei HB, Cai JS, Fan XY, Yang FZ, Sun SG (2007) Fabrication and properties of macroporous tin–cobalt alloy film electrodes for lithium-ion batteries. J Power Sources 170:450−455.
11. Fan XY, Ke FS, Wei GZ, Huang L, Sun SG (2008) Microspherical Cu_6Sn_5 Alloy Anode for Lithium-Ion Battery. Electrochem Solid-State Lett 11:A195−A197.
12. Kotobuki M, Okada N, Kanamura K (2011) Design of a micro-pattern structure for a three dimensionally macroporous Sn–Ni alloy anode with high areal capacity. Chem Commun 47:6144−6146.
13. Zhuo K, Jeong MG, Shin MS, Chun WW, Bae JW, Yoo PJ, Chung CH (2014) Morphological variation of highly porous Ni–Sn foams fabricated by electro-deposition in hydrogen-bubble templates and their performance as pseudo-capacitors. Appl Surf Sci 322:15−20.

14. Uysal M, Cetinkaya T, Alp A, Akbulut H (2015) Active and inactive buffering effect on the electrochemical behavior of Sn–Ni/MWCNT composite anodes prepared by pulse electrodeposition for lithium-ion batteries. J Alloys Compd 645:235−242.
15. Wada T, Yamada J, Kato H, Preparation of three-dimensional nanoporous Si using dealloying by metallic melt and application as a lithium-ion rechargeable battery negative electrode. J Power Sources 306:8−16.
16. Zhang J, Zhan Y, Bian H, Li Z, Tsang CK, Lee C, Cheng H, Shu S, Li YY, Lu J (2014) Electrochemical dealloying using pulsed voltage waveforms and its application for supercapacitor electrodes. J Power Sources 257:374−379.
17. Joshi MK, Pant HR, Tiwari AP, Kim H.J, Park CH, Kim CS (2015) Multi-layered macroporous three-dimensional nanofibrous scaffold via a novel gas foaming technique. Chem Eng J 275:79−88.
18. Zhou C, Yang K, Wang K, Pei X, Dong Z, Hong Y, Zhang X (2016) Combination of fused deposition modeling and gas foaming technique to fabricated hierarchical macro/microporous polymer scaffolds. Mater Des 109:415−424.
19. Xue LJ, Xu YF, Huang L, Ke FS, He Y, Wang YX, Wei GZ, Li JT, Sun SG (2011) Lithium storage performance and interfacial processes of three dimensional porous Sn–Co alloy electrodes for lithium-ion batteries. Electrochim Acta 56:5979−5987.
20. Arai S, Kitamura T (2014) Simple Method for Fabrication of Three-Dimensional (3D) Copper Nanostructured Architecture by Electrodeposition. ECS Electrochem Lett 3:D7−D9.
21. Nie M, Abraham DP, Chen Y, Bose A, Lucht B.L (2013) Silicon Solid Electrolyte Interphase (SEI) of Lithium Ion Battery Characterized by Microscopy and Spectroscopy. J Phys Chem C 117:13403−13412.
22. Nguyen CC, Lucht BL (2014) Comparative Study of Fluoroethylene Carbonate and Vinylene Carbonate for Silicon Anodes in Lithium Ion Batteries. J Electrochem Soc 161:A1933−A1938.
23. Courtney IA, Tse JS, Mao O, Hafner J, Dahn JR (1998) Ab initio calculation of the lithium-tin voltage profile. Phys Rev B 58:15583.
24. Shimizu M, Usui H, Matsumoto K, Nokami T, Itoh T, Sakaguchi H (2014) Effect of cation structure of ionic liquid on anode properties of Si electrodes for LIB. J Electrochem Soc 161:A1765−A1771.

25. Shimizu M, Usui H, Sakaguchi H (2016) Functional ionic liquid for enhancement of Li-ion transfer: Effect of cation structure on charge−discharge performance of $Li_4Ti_5O_{12}$ electrode. Phys Chem Chem Phys 18:5139−5147.
26. Yamada Y, Iriyama Y, Abe T, Ogumi Z (2010) Kinetics of Electrochemical Insertion and Extraction of Lithium Ion at SiO. J Electrochem Soc 157:A26−A30.
27. Wu H, Chan G, Choi JW, Ryu I, Yao Y, McDowell MT, Lee SW, Jackson A, Yang Y, Hu L, Cui Y (2102) Stable cycling of double-walled silicon nanotube battery anodes through solid-electrolyte interphase control. Nature Nanotech 7:310−315.
28. Gauthier M, Mazouzi D, Reyter D, Lestriez B, Moreau P, Guyomard D, Roué L (2013) A low-cost and high performance ball-milled Si-based negative electrode for high-energy Li-ion batteries. Energy Environ Sci 6:2145−2155.

Figure captions

Figure 1 (a) Scheme showing preparation of three-dimensional (3D)-Cu/Sn composite by an electrochemical process. (b) Photographs of Cu foil, 3D-Cu substrate, 3D-Cu/Sn prepared by electrodeposition using 0.25 M $Sn_2P_2O_7$ + 1 M $K_4P_2O_7$ + 0.005 M HCHO + 1.2 g dm^{-3} PEG-600, and Flat-Cu/Sn. (c) XRD patterns of 3D-Cu before and after electrodeposition of Sn.

Figure 2 Optical image of three-dimensional (3D)-Cu and flat-Cu substrates, and height profile analyzed by confocal scanning laser microscopy. The root mean square roughness (R_{rms}) was 0.835 for 3D-Cu and 0.087 for flat-Cu.

Figure 3 Kr adsorption isotherm of 3D-Cu prepared by an electroplating method using PAA additive.

Figure 4 FE-SEM images of 3D-Cu substrate (a) before and (b) after Sn-deposition with an energization amount of 3C. a_2-b_2 and a_3-b_3 are enlarged views of a_1-b_1 and cross-sectional images of the 3D-Cu and 3D-Cu/Sn electrode.

Figure 5 (a) Initial charge−discharge (Li-insertion/extraction) curves of 3D-Cu/Sn composite in 1 M $LiPF_6$/EC:DEC (50:50 vol.%). For comparison, the profile of Sn-film (Flat-Cu/Sn) electrode is also shown. The electrode was prepared by electrodeposition of Sn on Cu-foil. (b) Differential capacity vs. voltage (dQ/dV) curve of 3D-Cu/Sn composite electrode.

Figure 6 Differential capacity vs. voltage (dQ/dV) profile of 3D-Cu/Sn composite electrode during discharge reaction. The curve was deconvoluted into four components associated with stepwise Li−Sn reactions using a Gauss function. The peaks at 0.52 V, 0.62 V, 0.77 V, and 1.25 V indicate Li-extraction from $Li_{22}Sn_5/Li_7Sn_2$, $Li_{13}Sn_5/Li_5Sn_2$, LiSn, and Li_2Sn_5, respectively.

Figure 7 (a) Impedance spectra of cells including 3D-Cu/Sn and Flat-Cu/Sn electrodes at the first cycle. Inset: Randles circuit used in this study for cell impedance analysis. (b) Dependence of discharge capacity and coulombic efficiency on cycle number for 3D-Cu/Sn composite and flat-Cu/Sn electrodes.

Figure 8 FE-SEM images of electrodes as prepared and after charge−discharge cycling in 1 M $LiPF_6$/EC:DEC. The electrodes are (upper) 3D-Cu/Sn and (lower) Flat-Cu/Sn, respectively.

Figure 9 Discharge curves of 3D-Cu/Sn and flat-Cu/Sn electrodes under various current densities. (1C rate corresponds to 990 mA g^{-1})

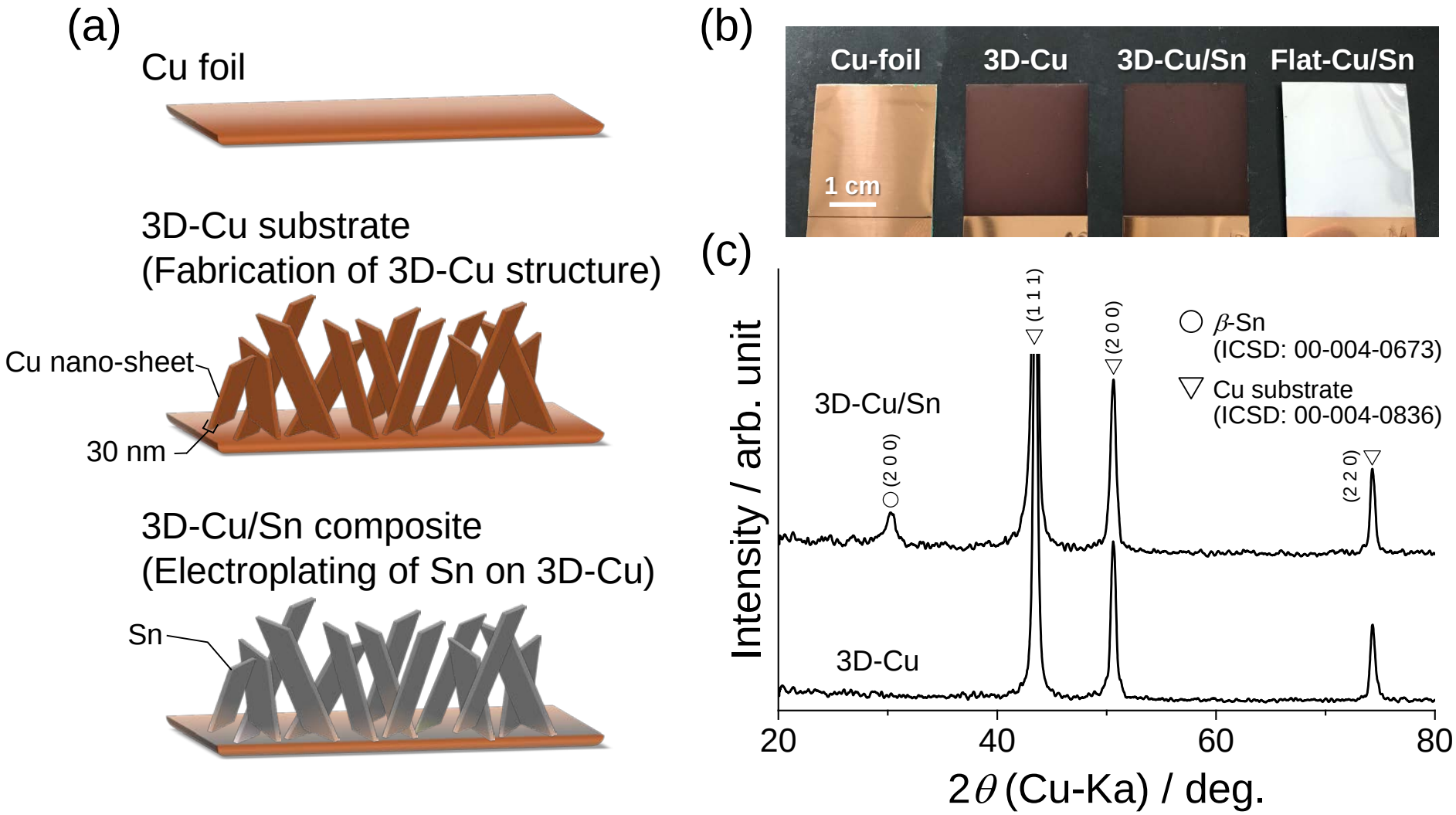

Figure 1 (a) Scheme showing preparation of three-dimensional (3D)-Cu/Sn composite by an electrochemical process. (b) Photographs of Cu foil, 3D-Cu substrate, 3D-Cu/Sn prepared by electrodeposition using 0.25 M $Sn_2P_2O_7$ + 1 M $K_4P_2O_7$ + 0.005 M HCHO + 1.2 g dm^{-3} PEG-600, and Flat-Cu/Sn. (c) XRD patterns of 3D-Cu before and after electrodeposition of Sn.

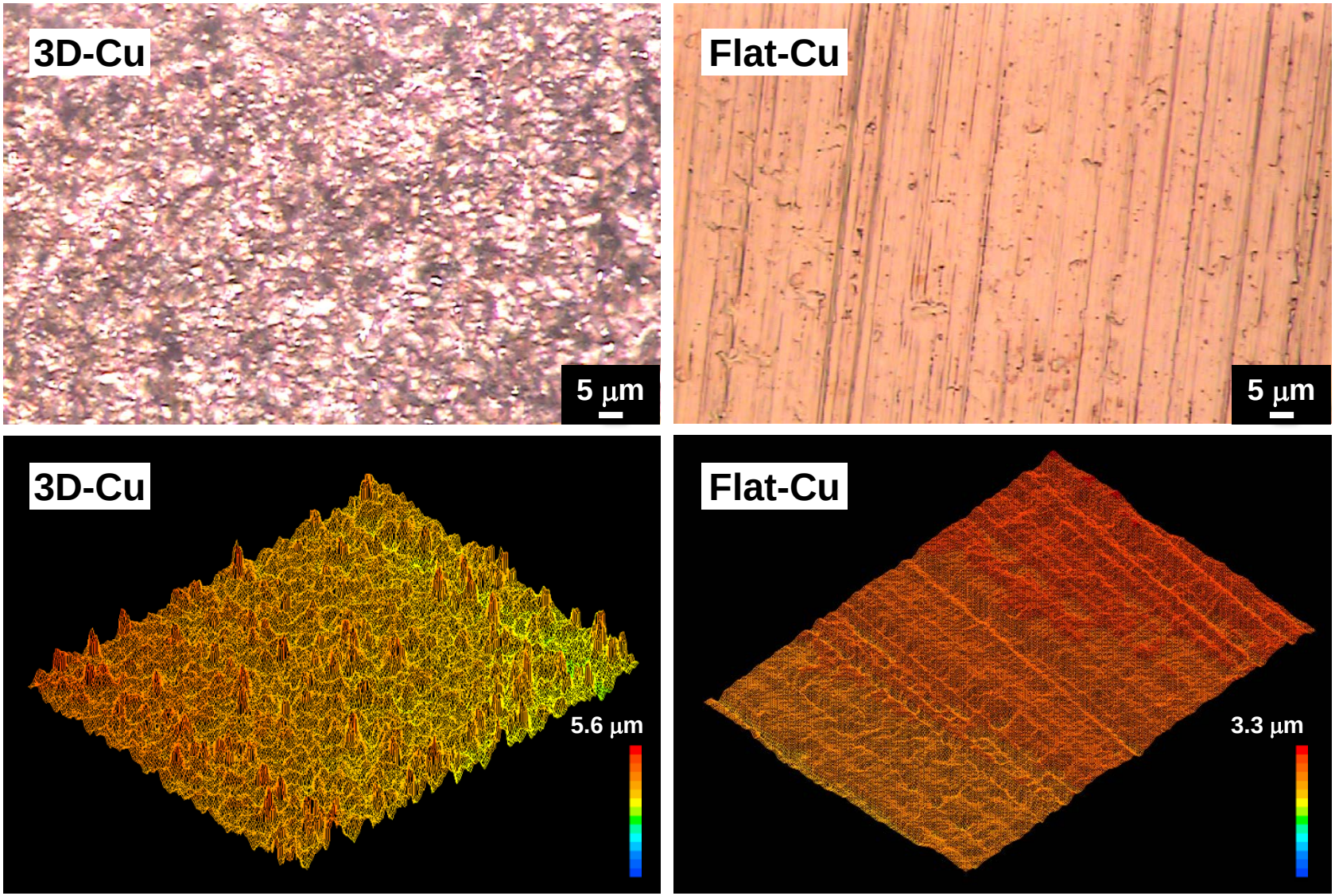

Figure 2 Optical image of three-dimensional (3D)-Cu and flat-Cu substrates, and height profile analyzed by confocal scanning laser microscopy. The root mean square roughness (R_{rms}) was 0.835 for 3D-Cu and 0.087 for flat-Cu.

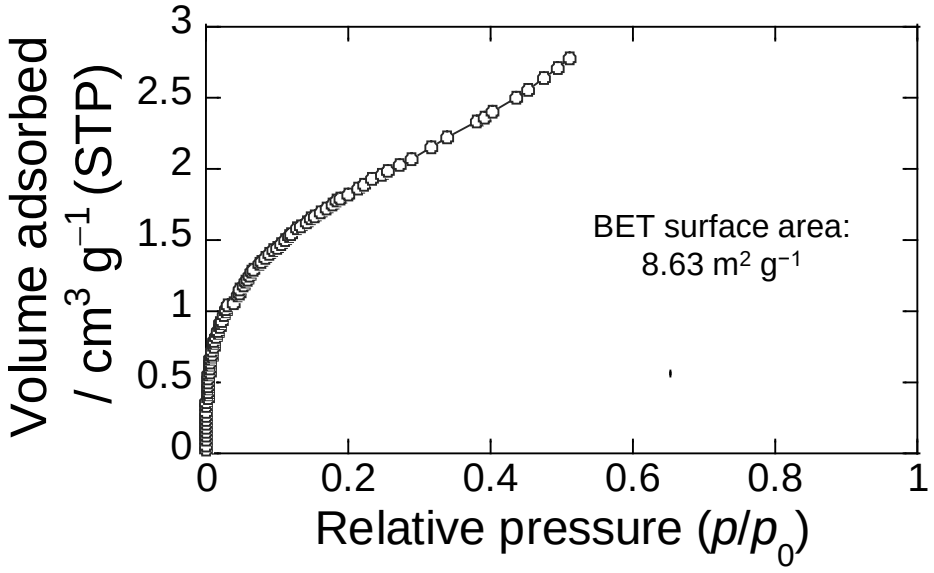

Figure 3 Kr adsorption isotherm of 3D-Cu prepared by an electroplating method using PAA additive.

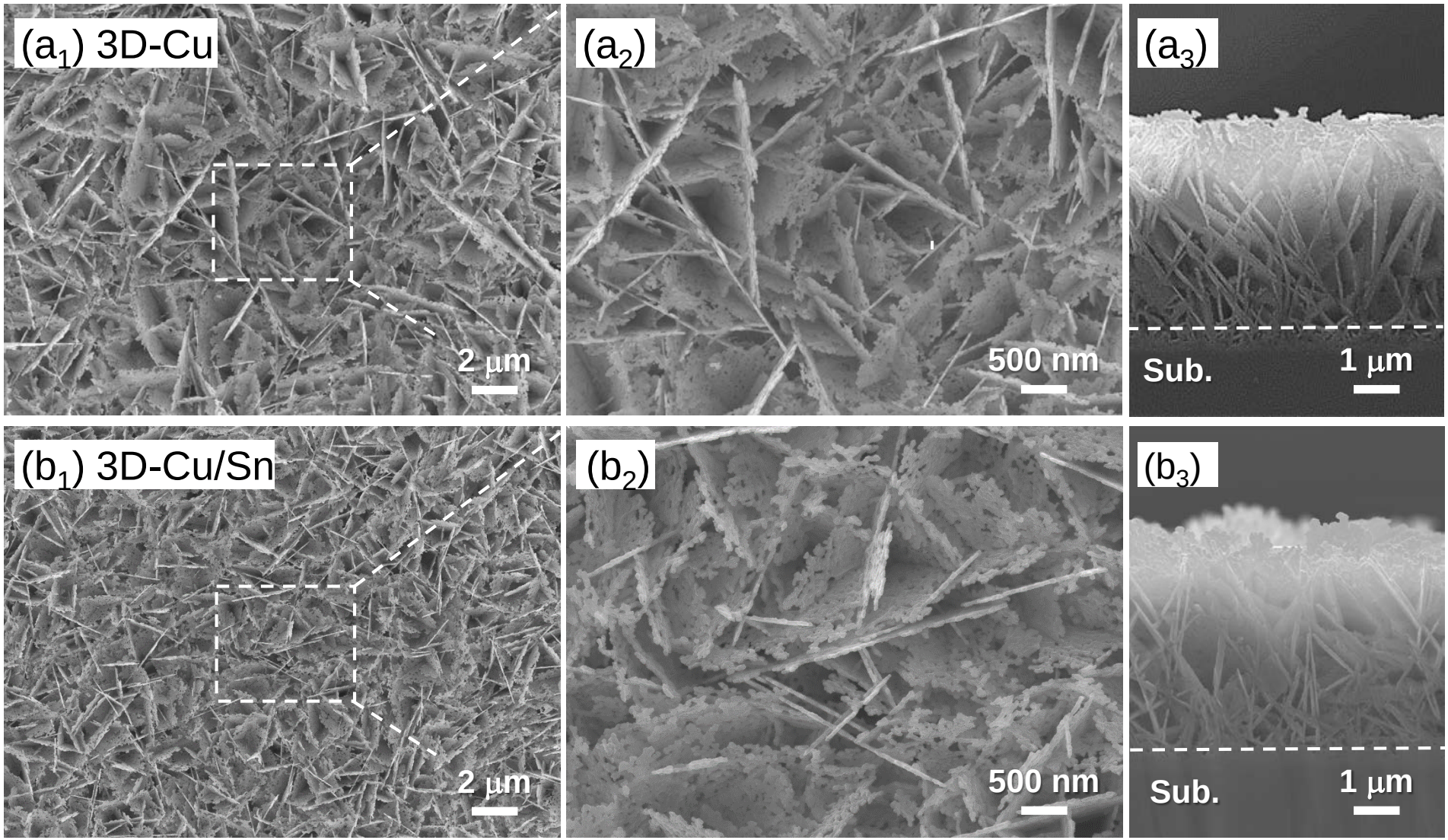

Figure 4 FE-SEM images of 3D-Cu substrate (a) before and (b) after Sn-deposition with an energization amount of 3C. a_2-b_2 and a_3-b_3 are enlarged views of a_1-b_1 and cross-sectional images of the 3D-Cu and 3D-Cu/Sn electrode.

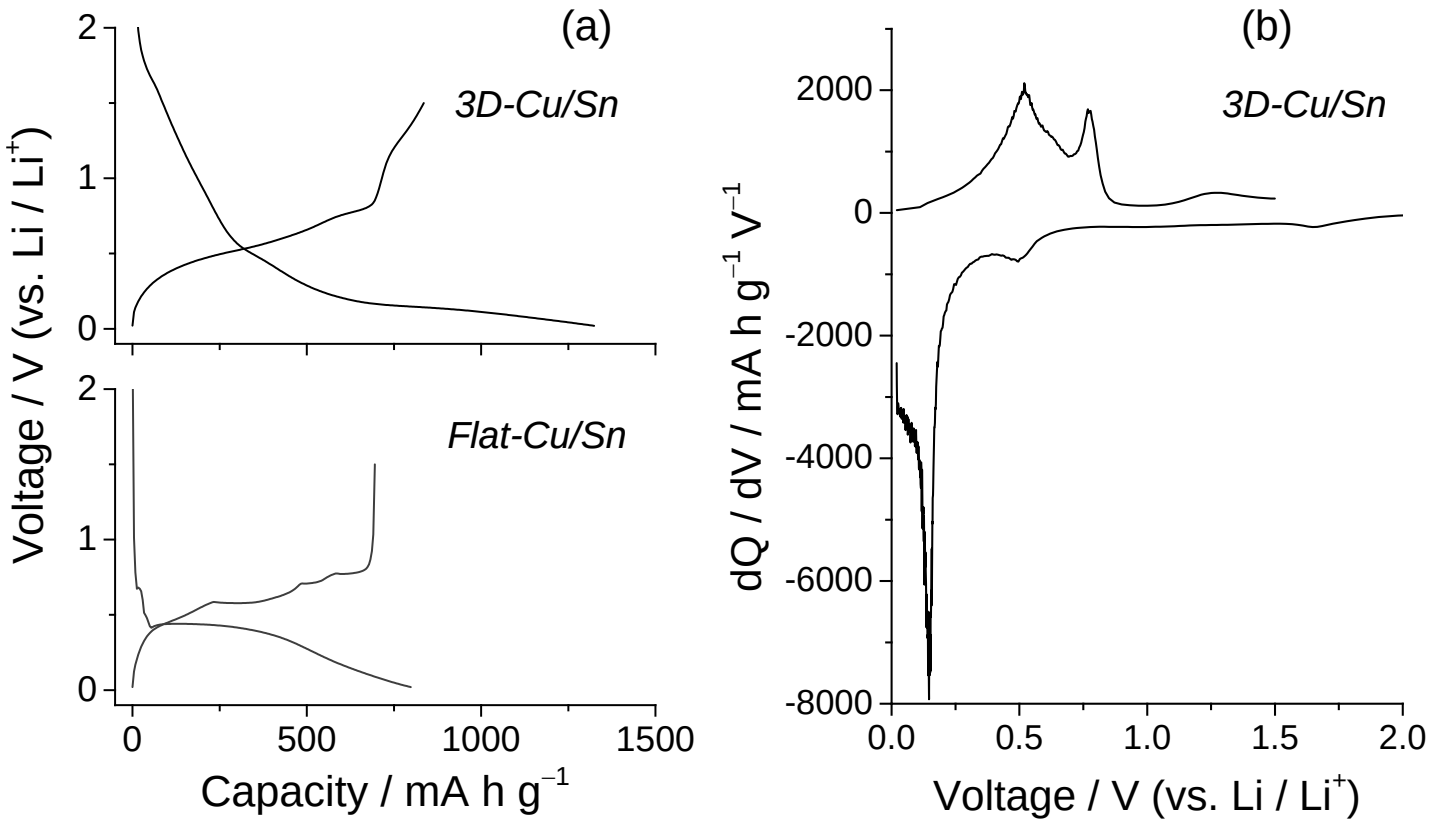

Figure 5 (a) Initial charge−discharge (Li-insertion/extraction) curves of 3D-Cu/Sn composite in 1 M $LiPF_6$/EC:DEC (50:50 vol.%). For comparison, the profile of Sn-film (Flat-Cu/Sn) electrode is also shown. The electrode was prepared by electrodeposition of Sn on Cu-foil. (b) Differential capacity vs. voltage (dQ/dV) curve of 3D-Cu/Sn composite electrode.

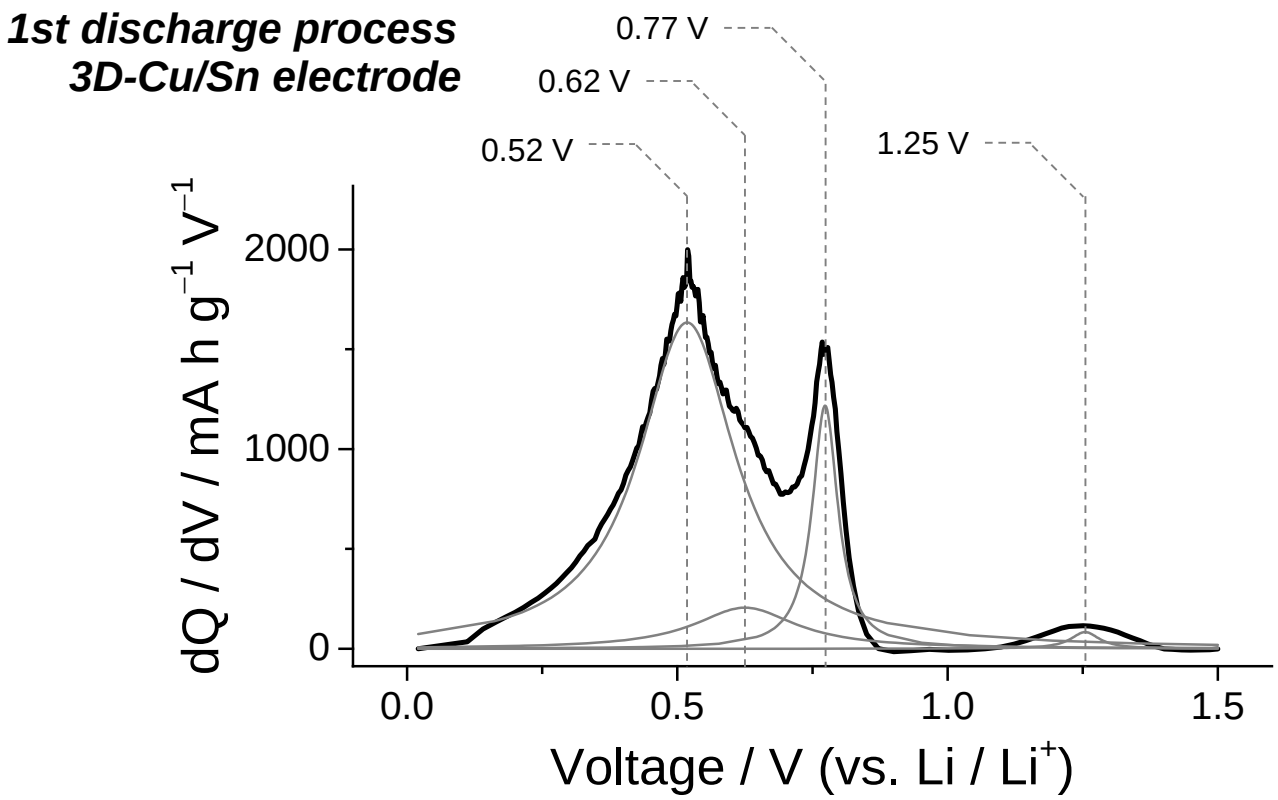

Figure 6 Differential capacity vs. voltage (dQ/dV) profile of 3D-Cu/Sn composite electrode during discharge reaction. The curve was deconvoluted into four components associated with stepwise Li−Sn reactions using a Gauss function. The peaks at 0.52 V, 0.62 V, 0.77 V, and 1.25 V indicate Li-extraction from $Li_{22}Sn_5/Li_7Sn_2$, $Li_{13}Sn_5/Li_5Sn_2$, LiSn, and Li_2Sn_5, respectively.

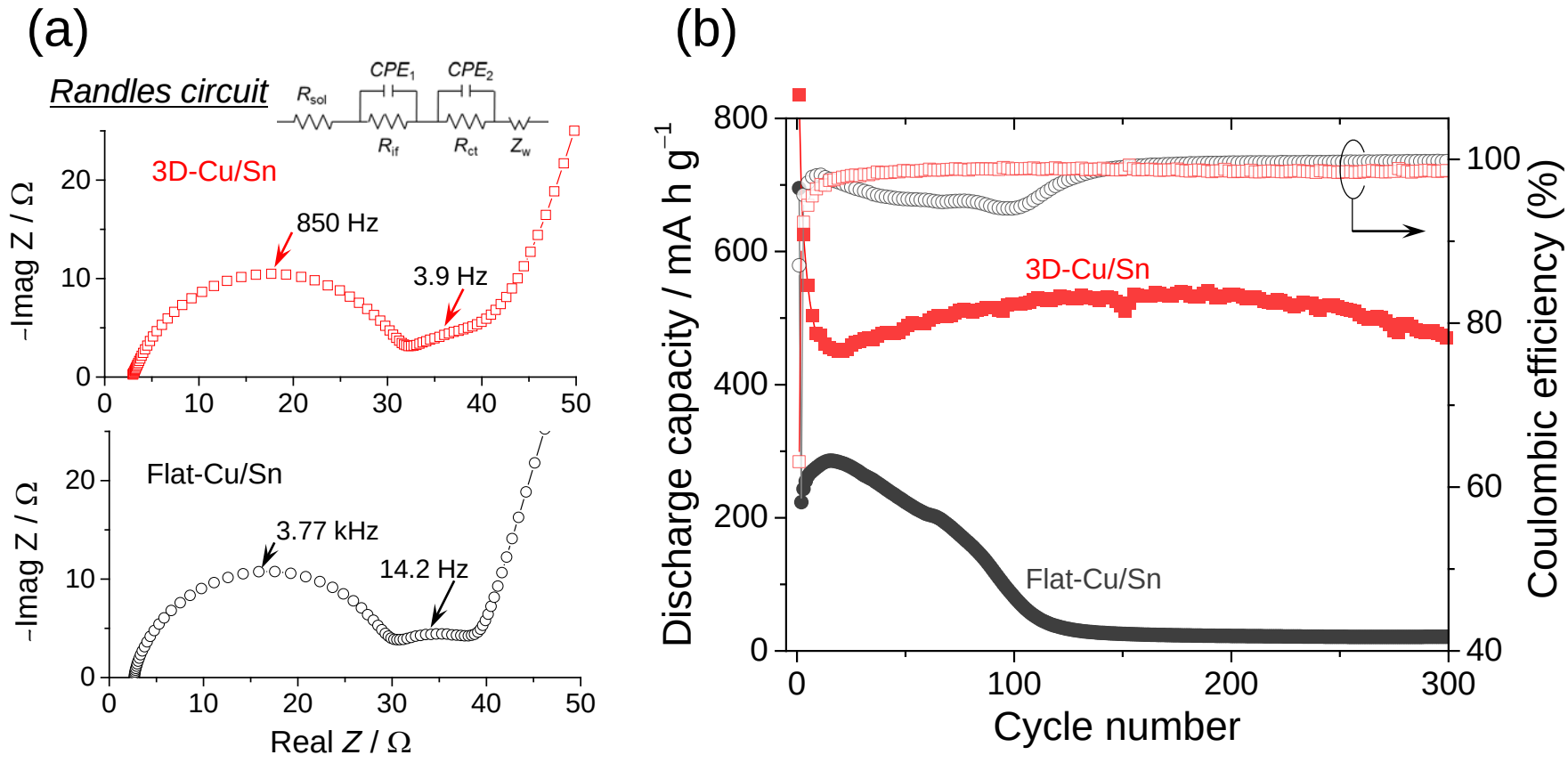

Figure 7 (a) Impedance spectra of cells including 3D-Cu/Sn and Flat-Cu/Sn electrodes at the first cycle. Inset: Randles circuit used in this study for cell impedance analysis. (b) Dependence of discharge capacity and coulombic efficiency on cycle number for 3D-Cu/Sn composite and flat-Cu/Sn electrodes.

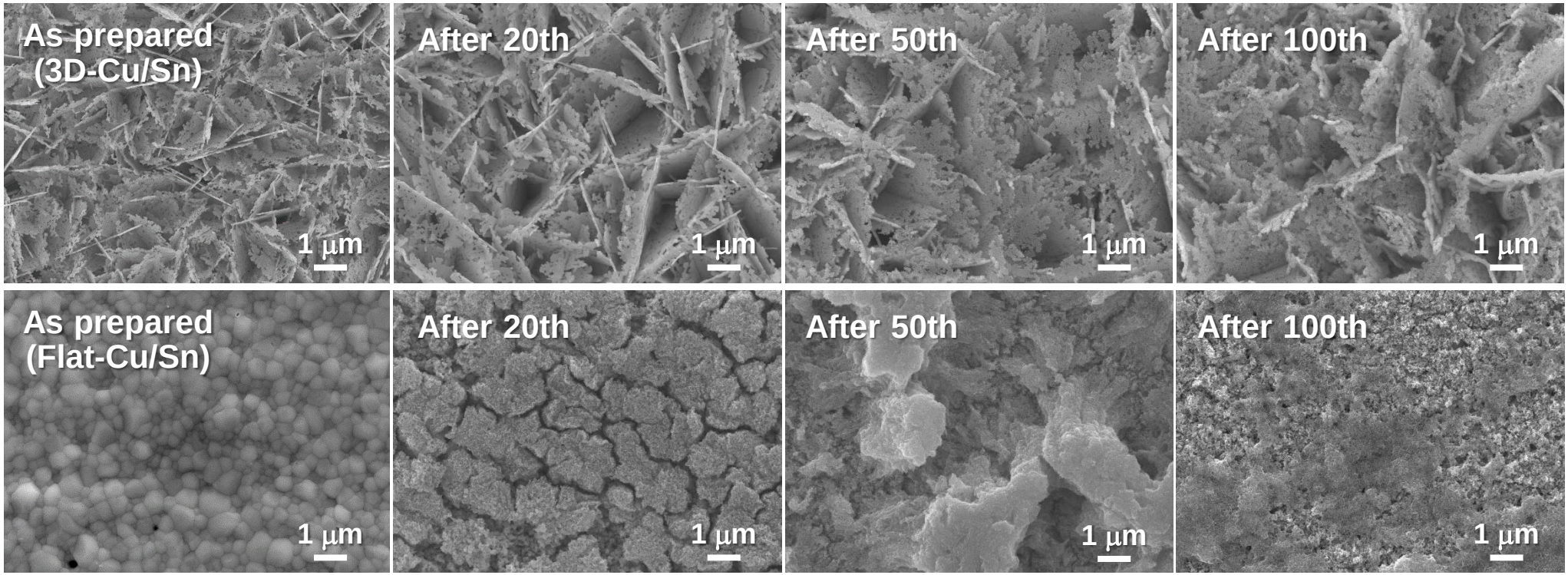

Figure 8 FE-SEM images of electrodes as prepared and after charge−discharge cycling in 1 M $LiPF_6$/EC:DEC. The electrodes are (upper) 3D-Cu/Sn and (lower) Flat-Cu/Sn, respectively.

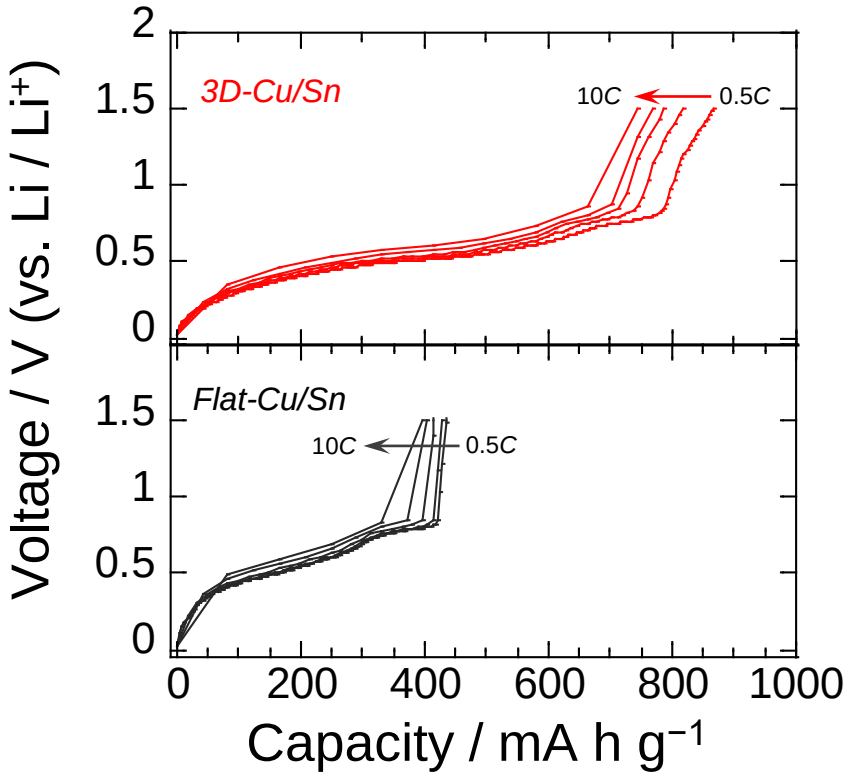

Figure 9 Discharge curves of 3D-Cu/Sn and flat-Cu/Sn electrodes under various current densities. (1*C* rate corresponds to 990 mA g^{-1})